Project no. 248992

Project acronym: NEUNEU

Project title: Artificial Wet Neuronal Networks from Compartmentalised Excitable Chemical Media

Small or medium-scale focused research project (STREP)

Deliverable 3.2 - Report for a Computational Model for Architectures Composed of Large Numbers of Droplets

This deliverable complements the link to experimental results and differential equation models from ICFPAN that were missing in deliverable D3.1.

Period covered: from 1.2.2010 to 31.1.2011 Date of preparation: 18.9.2009

Start date of project: 1.2.2010 Duration: 36 months

Project coordinator name: Dr. Peter Dittrich
Project coordinator organisation name: Friedrich Schiller University Jena

Multi-scale Modelling of Computers made from Excitable Chemical Droplets

Gerd Gruenert, Jan Szymanski, Julian Holley, Gabi Escuela, Alexandra Diem, Bashar Ibrahim, Andrew Adamatzky, Jerzy Gorecki, Peter Dittrich

February 28, 2012

Abstract

Here we review and extend models on different scales for a computing architecture made from networks of excitable chemical droplets. The model system of the Belousov-Zhabotinsky (BZ) reaction enclosed in lipid-coated droplets in oil is used to study signal transmission dynamics of chemical computers and their modelling. The excitable medium oscillates in the sub-excitable, excitable or self-exciting regimes, leading to excitation pulses that spread over the medium and can be used for information processing. We review a homogeneous differential equation model, the spatially extended partial differential equation model and a cellular automaton model of the chemical reaction and propose a new high level modelling approach for the droplets, which uses discrete states and potentially stochastic transition functions to represent the complex chemical state of each droplet. We show how the parameters like oscillation periods, diffusion coefficients and wave propagation speed for the models can be deduced from the lower level models and from experimental data. Furthermore we offer an outlook on the currently ongoing work and the role of the different modelling and simulation scopes within.

1 Introduction

Chemical computers might be used in many fields of applications, ranging from controlling bioreactors to designing smart drugs, as reviewed in [14, 13, 48].

In this article, we focus on modelling and simulation of compartmentalised, excitable chemical media for computation. An excitable medium, for example accommodating the Belousov-Zhabotinsky (BZ) reaction [47, 34, 1], can oscillate - either temporally or temporally and spatially - for many periods while consuming energy from the chemical substrate. Different media compositions generate qualitatively different behaviour: When the medium is in the *excitable* regime, it is able to oscillate for one period, once it is stimulated, but it will not spontaneously enter a new oscillation phase but return to the quiescent state. *Self-exciting* medium, in contrary, will start oscillating spontaneously. However, this medium can still be used for information processing, since new oscillation waves can also be triggered externally before the self-excitation happens. A more complicated behaviour is shown by a *sub-excitable* medium, that is basically less excitable than the initially mentioned *excitable* medium. That is, an excitation wave entering a droplet from one direction will not spread in any direction but will keep a "memory" of its direction. Also, when two *sub-excitable* waves collide, the resulting wave will propagate into a new direction, rendering this medium suitable for collision-based computing [2, 3, 25].

In our case, the BZ medium is compartmentalised into small droplets [8, 41] that form, when the medium is dripped into oil. The compartments are stabilised against merging through lipid molecules that self-assemble at the border between the aqueous and the oil phase. Where two droplets meet, a lipid double layer membrane can be formed that still allows chemical reagents to pass through and to trigger an excitation in the neighbouring droplet.

Based on a small experimental system of four droplets, we are giving an overview on the simulation techniques to describe and understand the behaviour of different kinds of Belousov-Zhabotinsky medium on different scales. After a short review of ordinary and partial differential equation and cellular automaton models, we introduce an event-based model that can be used to simulate a droplet network on large spatial and temporal scales. To motivate the requirement for distinct modelling scales, we give an overview on finished and ongoing work in the NEUNEU project[1] and explain how the modelling is applied therein.

[1] www.neu-n.eu

1.1 Principal Properties of the Belousov-Zhabotinsky Medium

The Belousov-Zhabotinsky (BZ) medium is a chemical mixture that can oscillate and be triggered into excitation. It is can easily be made by mixing sodium bromate, malonic acid, potassium bromide and ferroin in sulfuric acid [18]. However the resulting process is rather complicated: it has even been modelled using 26 chemical species and 80 reactions [24], so some kind of simplification is necessary for understanding the system. We will first summarise those aspects of the reaction that we will focus on in this work.

Most obviously, the BZ system exhibits different phases [15, 22, 17, 4]. A chemical redox indicator like forroin can provide information on the phase of the reaction system by switching from red to blue when a high concentration of reduced catalyst is outweighed by oxidised catalyst.

These phases, as visualised in Figure 1, show up under well-stirred conditions or with spatial resolution. Beginning in the *responsive phase* when the medium looks red, it can be triggered into an excitation or self-excite, displaying an almost immediate change from red to blue colour. When the fast change occurs, the medium is in the *excited* phase shortly and becomes *refractory* directly afterwards, rendering it unresponsive against further stimulation. Then the system recovers its red colour relatively slow and becomes ready for the next oscillation cycle. Once the BZ medium can be excited again, either by the excitation in the neighbourhood or through external influences, we shall refer to the medium as *responsive* here. Dependent on the type of medium, the *responsive* phase can be quite stable and last until some perturbation occurs. In case of the *self-exciting* BZ mixture, in contrast, the *responsive* phase can be instable such that a new oscillation cycle is started after the system was *responsive* for some time.

Excited droplets can influence their neighbours, but these can only react with a new excitation if they are in the *responsive* phase. When a droplet is *excited* we assume its oscillation can not be influenced by neighbouring *excited* droplets. But even when a droplet triggers its neighbour into a new oscillation, there will be some delay between the excitation of one and the next droplet, since the BZ waves will first have to cover some distance from one BZ compartment through the membrane and into the other droplet.

We analyse the system states in different areas of an exemplary BZ system of four linearly arranged droplets in Section 2 and estimate their oscillation periods and wave propagation speeds. Even though the chemical reaction process of the BZ medium is an inherently stochastic process and subject to random perturbations, the excitation periods of the droplets appear to be quite reliable. Nevertheless, there are qualitative changes happening in

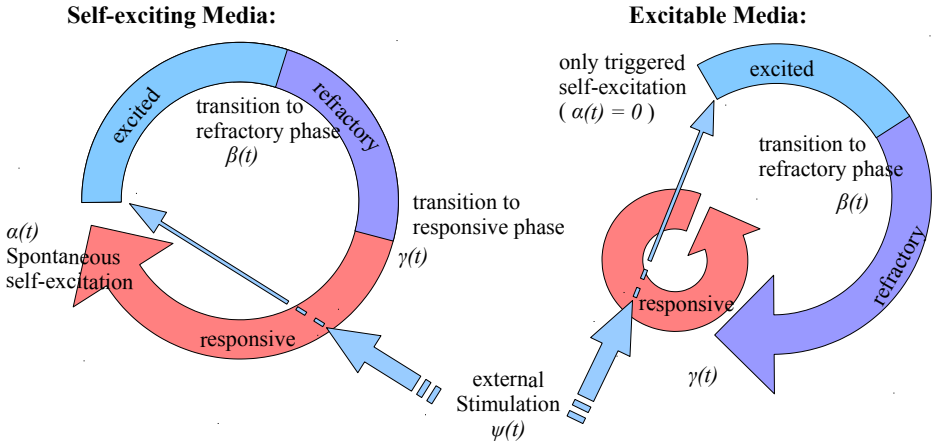

Figure 1: Abstract BZ Reaction cycle for self-exciting and excitable media. The complex Belousov-Zhabotinsky reaction can coarsely be described as a cyclic change of chemical conditions on the left side. For the *excitable* medium, the system can wait for external stimuli very long without going through an oscillation cycle by itself. The distribution functions $\alpha(t), \beta(t)$, $\gamma(t)$ and $\psi(t)$ describe the probability distributions for changing from one system state to another after staying there for time t.

the medium that are beyond the scope of our modelling, e.g. the continuous degradation of the medium and the concomitant increase of the oscillation periods. Furthermore, spiral waves [44, 22] form and disappear, maybe due to gas bubbles or spatial changes in the droplet structure. Though our models do not cover the genesis of these phenomena, we were able to describe the situation once the special conditions are established.

1.2 Hypothetical Droplet Types

Like specialised electronic components on a circuit board, we suggest to utilise a variety of specialised droplet types. The "normal" droplets, that we were describing so far and that we are considering in this paper's experiments and models, can be characterised as *Or* droplets: when we consider droplet "crossroads", where a droplet is connected to three or four other droplets, a signal arriving on one lane will spread out in all other directions as long as the other droplets are *responsive*. Nonetheless, we will introduce some hypothetical droplet types that can be of use when designing more complex droplet computers as pointed out in the Outlook Section 5.

Or The standard droplets as we are describing them in Sections 2 and 3. These droplets distribute incoming excitations to all other adjacent and *responsive* droplets. If there are two inputs to a droplet of this type, both inputs can equally lead to an excitation, such that the droplet behaves like a logical "And".

High Activity A droplet that is filled with quickly oscillating, self-excitatory medium might be used to supply a droplet network with continuous signals, e.g. acting as pacemaker or timing signal. It is possible to manufacture this kind through a different BZ medium composition or by externally influencing the droplet, for example via optical stimulation.

And Droplets that can be stimulated by two or more synchronously arriving excitation waves, but not by a single one, might be build from droplets that contain less excitable BZ mixture. It is an open question, dependent on the further exploration of the droplets in laboratory experiments, how much synchronisation between the two input signals is necessary to allow an activation of the *And* droplet.

Diode Another possibly valuable droplet type can propagate signals solely in a single direction while blocking signals arriving from the other direction. It could thus help to insulate some parts of a droplet network from the influences of other substructures and in general to have more control

species	concentration
sulphuric acid	0.6 M
sodium bromate (NaBrO3)	0.45 M
malonic acid	0.35 M
potassium bromide (KBr)	0.06 M
ferroin	1.7 mM

Table 1: Composition of the BZ medium.

over the range of system dynamics. A chemical implementation can be achieved using diode membrane channels [31], through differently sized droplets [39, 41] and probably also with a different media composition.

Repeater To solve potential timing problem of the *And* Droplets, we assume that we can manufacture a *repeater* droplet that will, once activated, repeat an excitation signal for longer than the typically short *excited* phase. This can be realised through droplets with different sizes [39] or medium compositions [21], resulting in different oscillation periods.

Inhibition A droplet that, once activated, inhibits its adjacent droplets might prove extremely helpful. One could argue that the oscillation in the inhibitory droplet might consume the substrate of its neighbour droplets or that it might throw its neighbours into the *refractory* state, bypassing the *excited* state. Even though this type of droplet might be hard to produce, we will still consider the implications of the theoretical existence of such a droplet.

2 Example System and Experimental Data Processing

We describe our modelling approaches by a system that consists of four stacked droplets of different sizes as displayed in Figure 2a. The droplets are filled with BZ medium of the composition summarised in Table 1. This leads to *self-exciting* oscillations, as predicted by the differential equation models (Section 3.1). The largest diameter of the droplets is approximately 10^{-3} m and the length of the droplet chain is approximately $6 * 10^{-3}$ m. Though the droplets in this system change their form slightly over time, the general structure and the droplets' linear arrangement stays constant over the experimental time of approx. 48 minutes or 2880 s (Supplementary movie 1)

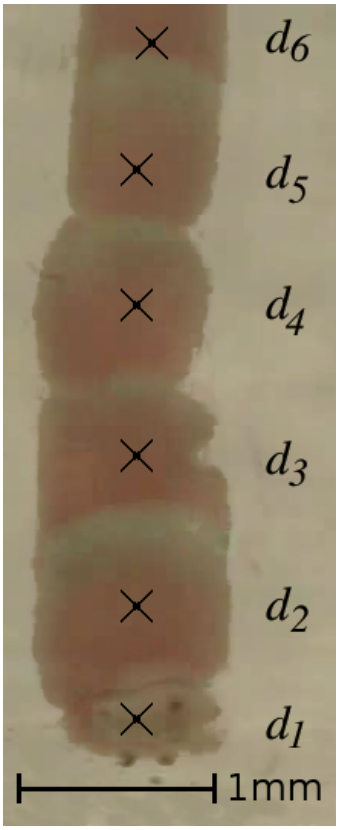

(a) droplet system

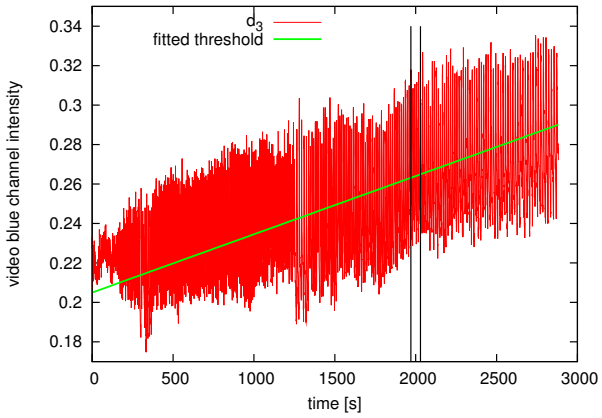

(b) position d_3

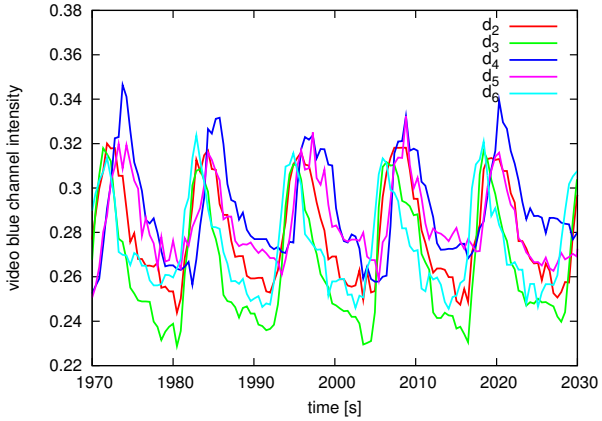

(c) all droplets

Figure 2: Droplet system and extracted oscillation data. a) Different positions along the droplet system are marked with the symbols d_1 till d_6. b) The excitation state of position d_3 is plotted over the whole experimental time. Additionally, a green line indicates the threshold that will later be used to extract oscillation periods from this data. Vertical black lines show the interval that is represented in Figure 2c. c) The intensities at the positions d_2 till d_6 are plotted over a small time window. Due to impurities and the small size of droplet d_1, we could not extract excitation data here.

By extracting the blue channel of the experiment video, we can observe the state of the complex BZ reactions in one dimension. The blue channel is extracted as the average of a 10 by 10 pixel rectangle around the six different positions marked in Figure 2a. The blue colour component of the video and thus the concentration of the oxidized catalyst over time is displayed in Figure 2b for the position d_3 only and in Figure 2c for all positions but over a smaller time frame. Probably due to impurities and due to the small size of the lowest droplet, we could not extract usable oscillation data for the position d_1.

From the oscillation data, we measured the oscillation periods that are displayed in Figure 3. The oscillation periods are determined by approximately overlaying a "threshold line" centrally over each of the oscillation plots analogous to the green line displayed in Figure 2b. Then the interval between the times when the threshold line is crossed upwards gives the oscillation periods for each position as displayed in Figure 3. In this figure, the main accumulation of oscillation periods increase linearly over the whole experimental time, starting from about 5 s and arriving at about 15 s oscillation period length. Some outlying points originated from the noise in the video data as seen in Figure 2c which leads to some positions being identified as rising oscillation flanks mistakenly. Likewise, some actually rising flanks may not be found, resulting in longer oscillation periods in the plot.

In a similar way, we calculate the interval between oscillations at neighbouring positions to estimate the delay of the excitation wave between these positions as displayed in Figure 4. The time delay for the wave propagation is not equal between all positions pairs. Nonetheless, this does not imply that the wave travels through the medium at different speeds. Instead, the positions are not exactly the same distances apart. Additionally, crossing the lipid membrane, e.g. between the positions (d_1,d_2), (d_3,d_4) or (d_4,d_5), does take the excitation wave longer than travelling the same distance inside a droplet, e.g. between the positions (d_2,d_3) or (d_5,d_6).

The system is observed for 2880 s, counting around 300 oscillations during this time. The system's oscillation periods are increasing almost linearly over the experiment as shown in Figure 3. Nevertheless we are using constant oscillation periods in all modelling scopes here, even though we are working at incorporating the dynamically changing system behaviour. Since the system showed a rich variety of different behaviours around the time $t_m = 1000\ s$, we chose this time for the modelling in the next section.

The lowest and smallest droplet at position d_1 with a diameter of about 0.6 mm oscillates the fastest and, for most of the time, controls the oscillations in the remaining system. Another interesting behaviour of the observed droplets is a phase of slower self-excitation of the top droplet at positions d_5

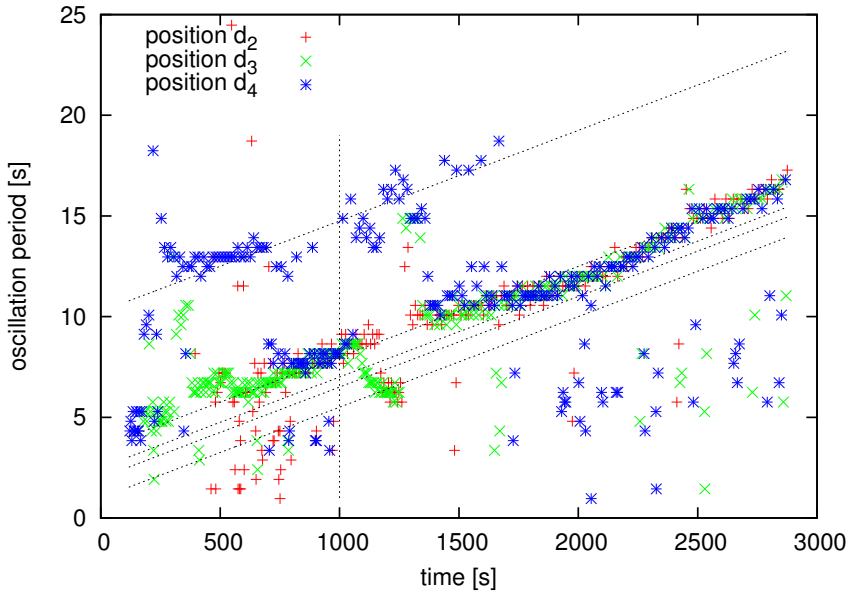

Figure 3: Oscillation periods extracted from experimental video. For simplicity, only positions d_2, d_3 and d_4 are shown in this plot. Generally, the oscillation periods increase over the experiment, following an approximately linear regime. A large cluster of oscillation periods is found on the line linearly climbing from 5 up to 15 s (second auxilary line). These oscillations are results of trigger waves originated at position d_1. Most of the time, as can be observed in supplementary video 1, these waves spread out and dominate the whole system. A second cluster of oscillations on the line from 10 up to 25 s is mostly observed in the first half of the experiment (first auxilary line). Here droplets self-excite because of broken influence of position d_1, supplying an estimate for the self-oscillation periods of droplets. Oscillations plotted below the lowest auxiliary line are most likely due to measurement and data extraction errors, such that two successive oscillations would often add up to elements on the main accumulations. As an exception, around the time 1200 s, a spiral wave pattern emerges close to position d_3 and leads to faster oscillations at position d_2 and d_3. Since these waves arrive with a high frequency, the BZ solution at the lipid bilayer between positions d_3 and d_4 does not have enough time to recover. Hence only every second wave can be transmitted over the gap between the droplets. Partially this long time between two oscillations already leads to self-excitations.

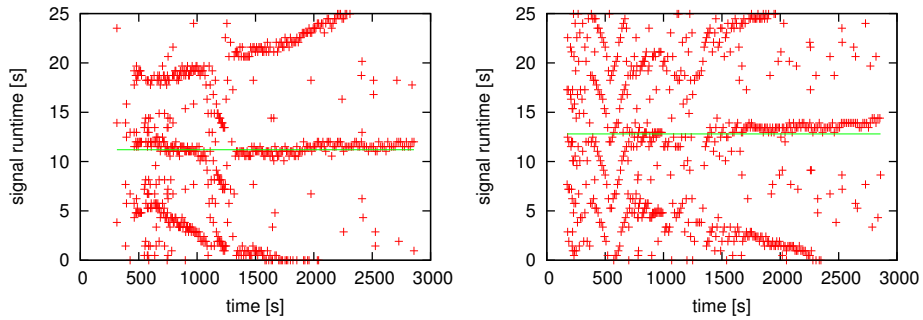

(a) positions d_2 and d_3

(b) positions d_3 and d_4

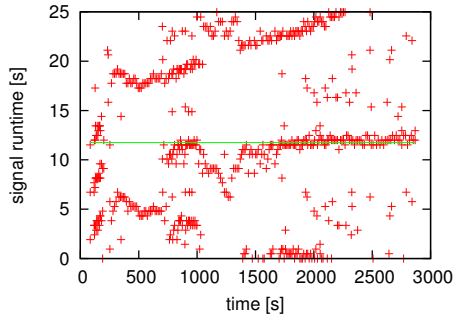

(c) positions d_4 and d_5

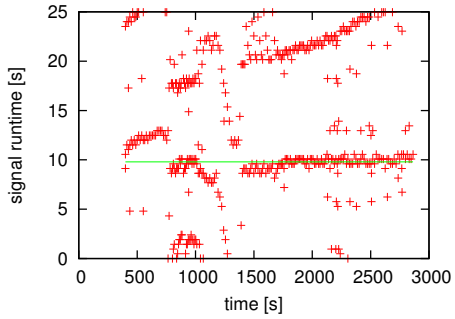

(d) positions d_5 and d_6

Figure 4: Signal propagation times, extracted from video data in Figure 2. The red crosses indicate the time delays between excitation of one droplet position and the following position. The green lines are fitted along the main aggregation of signal propagation times around 10 s and is used to parameterise the delay times of the discrete-event model in Section 3.4. The aggregations of delay times around 10 s are caused by a single excitation wave passing the system in forward direction, i.e. from d_i to d_{i+1}. The other two major aggregations, which are increasing and decreasing over the experimental time, are caused by waves that pass position d_i before or after the wave that is considered for position d_{i+1}. While the wave propagation speed stays approximately constant over the experiment, the delay between two successive waves at two distinct positions changes with the oscillation frequency over the experiment, leading to the increasing and decreasing secondary aggregations in the plots. In the time window between times 1000 s and 1500 s, the direction of the waves is partially inverted, leading to a change in the measured time delays as well. Furthermore, there are some delays marked far-off the main aggregations, which are mostly a result of mistakes at identifying the rising flanks of the oscillation due to noise.

system property	**observation timeframe**	**position**	**fitted function**
trigger-wave from d_1 period	200 .. 2880 s	d_1 .. d_6	$\frac{9}{2000}t + 3.5\ s$
self-excitation period	500 .. 1500 s	d_2 .. d_6	$\frac{9}{2000}t + 10.25\ s$
refractory time, lipid bilayer	1200 s	d_3, d_4	$\frac{9}{2000}t + 2\ s$
oscillation period, spiral wave	1230 s	d_3, d_2	$\frac{9}{2000}t + 1\ s$

Table 2: Summary of the functions that are fitted based on Figure 3. The fit of the trigger waves' oscillation period, which control the system most of the time, is obvious. Fitting the self-excitation times that can be observed between times 500 till 1500 s is harder because of the smaller number of samples and a large variance therein. Choosing a linear function with the same slope as the trigger-wave function leads to an acceptable fit, at least in the small time window that the self-oscillations appear in. For the remaining parameters, the refractory times of droplet centres, droplet borders and the oscillation times of spiral waves, there is basically just one point along the time axis available. So following the previous two functions, we assumed the same slope again here. Nonetheless, for modelling the system behaviour around time $t = 1000\ s$, the error should be relatively small because the underlying observations are made close to this time as well.

and d_6 in a time window between simulation time 300 s and 800 s. In this phase, the top droplet self-excites with an oscillation period that is longer by a factor of about 2, compared to the oscillations induced by the lowest droplet at position d_1. There is also a short abnormal phase between the times 1050 s and 1250 s when a spiral forms in the lower middle droplet and leads to an oscillation period that is reduced by a factor of approximately 0.7, compared to the triggered oscillations. While these fast oscillations propagate into the lowest droplet after some time, they do not cross the membrane to position d_4 and above. These observations allow us to characterise the behaviour of the droplets as summarised in Table 2.

3 Modelling Excitable and Self-Exciting Droplets

For model building, there are typically versatile approaches available that influence model characteristics like the level of detail, the accuracy, the simplicity, computability and other features. Differential equation approaches are often based on first principles, highly detailed but mostly also computationally demanding. They are probably best suited for understanding the behaviour of the BZ reaction, especially when happening under uncommon conditions like inside a lipid membrane with its side effects. This understanding is the basis for optimising the chemical composition of medium, oil and lipids to produce a desired behaviour.

But for figuring out which kinds of behaviour could actually be of use to perform some kind of computation, faster and larger models including hundreds and more droplets become necessary. This is for example the case with cellular automaton or event-based simulation models of droplets that are simplified to use discrete states instead of continuous concentrations. In an even more abstract sense we will also need modelling techniques, such as high level programming languages to describe the function of complex droplet networks. We will give a short outlook into this direction in Section 5.

Naturally, the further one of these modelling viewpoints is apart from the first principles of the system, the harder will it be to obtain the necessary parameters. Ideally, we would like experiments and first principle models to parameterise the models on the next abstraction level. In contrast here, some of the higher level properties such as oscillation periods and wave propagation velocities can be observed directly in the experiment.

3.1 Well-Stirred Ordinary Differential Equation Model

Starting with the local BZ medium behaviour, i.e. without considering diffusion, the most prominent models are the Brusselator [37] and the Oregonator [34, 15] models using ordinary differential equations. We are using variations of these model by Szymanski et al. [41] and Gorecki et al. [21], that allow obtaining the necessary system parameters directly from the experimentally used concentrations [41, 21, 18]. In the simplified two variable interpretation, the model describes the dynamics of one activating chemical species x and one repressing chemical species z. They correspond to bromous acid ($HBrO_2$) and ferroin ($Fe(phen)_3^{3+}$) concentrations, respectively. It reads as

follows:

$$\frac{\partial x}{\partial t} = \epsilon_1 h_0 N x - \epsilon_2 h_0 x^2 - 2\alpha\epsilon_1 MK \left(\frac{1}{\beta} + q\frac{1}{h_0}\frac{z}{1-z}\right)\frac{x-\mu N}{x+\mu N} \tag{1}$$

$$\frac{\partial z}{\partial t} = \frac{h_0 N}{C}x - \alpha\frac{KM}{Ch_0}\frac{z}{1-z} \tag{2}$$

The necessary model parameters are h_0: the Hammett acidity function of the solution and the concentrations of $K : \mathrm{KBr}$, $M : \mathrm{CH_2(COOH)_2}$, $N : \mathrm{NaBrO_3}$ and the catalyst $C : [\mathrm{Fe(phen_3^{2+})}] + [\mathrm{Fe(phen_3^{3+})}]$ as listed in Table 1. Further fixed parameters are $\mu = 1.6 * 10^{-5}, \alpha = 2.6 * 10^{-4}, \epsilon_1 = 1200, \epsilon_2 = 6700, \beta = 1000$ and $q = 0.51$.

The oscillation cycle, cf. Figure 1, starts the *excited* phase with a moderate concentration of the activator x and a low concentration of the repressor z. Then the amount of repressor and activator rise rapidly and lead to a negative second derivative $\frac{dx}{dt}$ for the activator equation until x will finally drop back to its initial low value. From this point on, we call the BZ solution *refractory* with a low activator concentration and high but slowly decreasing repressor concentration z.

Now, if there was a small inflow of activator into the system, the BZ mixture could not be triggered into the next oscillation because the high repressor concentration would quickly degrade the activator. But when the repressor concentration z drops below a critical value, an inflow of activator x will not be degraded fast enough and the BZ mixture can be triggered into a new oscillation cycle. We define the *responsive* phase such that it begins when a specific activator inflow is sufficient to trigger the next excitation in the BZ mixture and lasts until the next *excited* state begins. Clearly the begin of the *responsive* state and thus the threshold for the concentration of the repressor z depends on the amount of activator that flows into the system. This inflow would typically stem from an arriving excitation wave when considering spatially inhomogeneous BZ mixtures. Hence it is not possible to describe this point without a characterisation of the membrane boundaries or the diffusion coefficients. In contrast, when using partial differential equations and appropriate diffusion coefficients in the next section, the inflow of activator from an arriving excitation wave is defined.

Dependent on the BZ system characteristics, the next *responsive* phase can last infinitely in the case of the *excitable* medium. Alternatively, the repressor can, in *self-excitable* medium, drop so low that the next excitation wave is triggered reliably after a certain interval.

3.1.1 Stability Analysis of the Well-Stirred Ordinary Differential Equations Model

Stability of a system can be determined by the crossing of its nullclines. The nullcline (or zero isocline) refers to the slope of a function which will always be the same (zero), regardless of the initial conditions. More precisely, assuming that the right-hand-sides of the nonlinear differential equations (Eqs. 1 & 2) are $f(x, z)$ and $g(x, z)$ respectively. Then, the x-nullcline is the set of all points in the x-z plane satisfying $f(x, z) = 0$. The z-nullcline is the set of all points satisfying $g(x, z) = 0$. Equilibrium points (or fixed points) are the intersection points of x-nullcline and z-nullcline. Hence, in this BZ system, there are potentially three fixed points (for the given parameter values). They are as (x, z) pairs: $P_1 = (-1.5 * 10^{-8}, -7 * 10^{-4})$, $P_2 = (6.9 * 10^{-5}, 0.97)$ and $P_3 = (-0.016, 1.0)$. To analyse the stability of these states (fixed points), we calculate analytically the Jacobian and evaluate its eigenvalues. These eigenvalues with respect to each fixed point are respectively: $(206.3, 0.16)$ an unstable Node, $(103.1, -4.6)$ a Saddle point and $(-60657.4, -4.4)$ a stable Node. Since, we are working on a chemical system, therefore solely the unstable Saddle fixed point $P_2 = (6.9 * 10^{-5}, 0.97)$ is realistic and relevant.

Next, any gradient system has no limit cycle and any close orbit. We tested the differential equation system and observed it is not gradient. That is the partial derivatives of the functions are equal to zero. That helps us to determine a limit cycle from our phase space plot (see phase space Figure 5 C & D). Subsequently, we simulated the differential equation model (t=300s) and scan all parameters individually and independently.

We found that high values (increasing the default given values) of α, μ, N, M and K lead to high (more) oscillations while low values of q, ϵ_2 or C lead to decrease oscillations.

Amplitude with respect to x is getting higher by increasing any of α, M and K and getting lower by increasing h_0 and ϵ_2. Amplitude with respect to z is getting higher when increasing h_0 and low z-amplitude can be reach by increasing α, ϵ_2, M and K. The system has no significant effect via changing ϵ_1. Interestingly, h_0 has a switching value around 0.0013. As long as h_0 belongs to the interval 0.000001 and 0.0013, oscillations decrease with increasing h_0. Once, h_0 becomes higher than 0.0013, oscillations increase with an increasing h_0 value. Furthermore, the h_0 value does not affect the amplitudes of the oscillations.

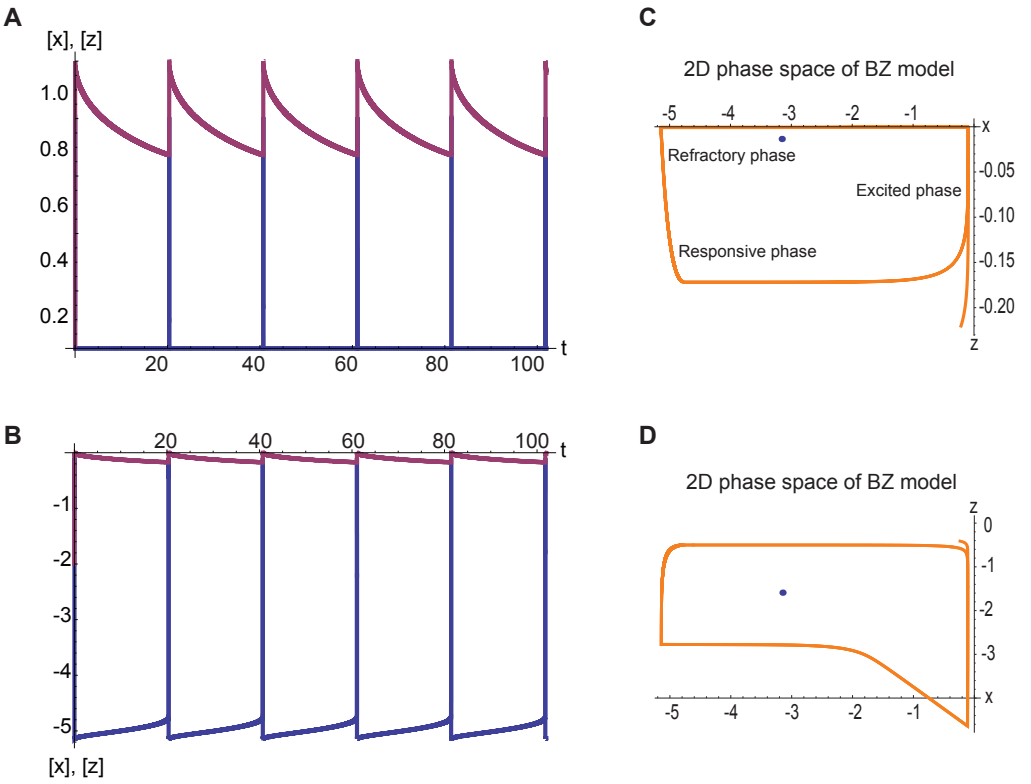

Figure 5: Numeric simulation and phase space of the BZ system trajectory. In plots A and B, blue denotes the concentration of the activator species x and purple the repressor species z. In comparison to plot A, plot B uses a logarithmic y-axis for a better observation of species x. Plots C and D show the phase space with logarithmic x-axis. The blue dot is the position of the system's fixed point. Since z moves very close to the $z = 1$ system boarder, plot D shows the same phase plot with additionally transformed z-axis to $z' = log(1 - z)$.

3.2 Reaction-Diffusion Partial Differential Equation Model

For describing the spatial and temporal propagation of excitation waves in addition to the well-stirred dynamics of the BZ system, we need to include space. In the simplest form, this can be done by adding the Laplacian term into differential equation (1) of system variable x that is supposed to diffuse [21, 18], arriving at equation (3). We consider the molecules represented by system variable z to be larger, leading to diffusion on a slower timescale that will be ignored here. This change introduces the diffusion coefficient D_x of species x as new parameter, resulting in the equations:

$$\frac{\partial x}{\partial t} = \epsilon_1 h_0 N x - \epsilon_2 h_0 x^2 - 2\alpha\epsilon_1 MK \left(\frac{1}{\beta} + q\frac{1}{h_0}\frac{z}{1-z}\right)\frac{x-\mu N}{x+\mu N} + D_x \triangle x \quad (3)$$

$$\frac{\partial z}{\partial t} = \frac{h_0 N}{C}x - \alpha\frac{KM}{Ch_0}\frac{z}{1-z} \quad (4)$$

The partial differential equation models of BZ droplets proved their value for investigating the interaction between two droplets [18] and, in a slightly modified form, for designing circuits or logic gates of about ten droplets for sub-excitable medium as we will show in Section 4.

Many parameters, such as diffusion coefficients for different species or at different locations in the droplet, might be hardly observable. Here, parameter fitting approaches are a practical way of deducing knowledge about the system from macroscopic properties like wave propagation velocities or oscillation periods [18]. On the downside, these parameter fitting methods are indirect and results are not guaranteed to be unique.

However, the spatial expansion of the ordinary differential equation model of the last section is not straightforward. Causes are the immense computational efforts of the simulation, numerical instabilities, diffusion properties through the lipid bilayer that have to be determined in addition to coefficients in the medium and boundary conditions at the droplet borders. For example in supplementary movie 1, the waves' passage over droplet borders and the resulting wave delay can be observed. Also, close to the droplet borders the BZ reaction can be repressed [39], whereas we assume a spatially homogeneous BZ medium in equations (3) and (4). Computations can be sped up using graphics card acceleration with CUDA [28] and by specialised simulation techniques [12]. Nonetheless, the numerical integration of such a partial differential equation system is computationally expensive and will mostly be used for small systems, considering few excitation waves.

3.3 Cellular Automaton Models

The problems of complex parameter sets and high computational expenses can at least partially be resolved in cellular automata [43, 45]. In this case, more phenomenological, *ad hoc* models are built, which rely on less unobservable parameters, but also less on first principles but rather on the observable properties of the system. Space is mostly discretised into a regular grid. Also time and cell states are discrete and update rules describe how each cell's state is calculated from the cell and its neighbourhood's previous state. The discretisation usually uses a varying number of states that fall into the classes of *excited*, *refractory* and *resting* or *responsive* phases. Examples for such automaton models could be four state systems [22] or three state automaton models [1, 4, 27] that were already used to simulate systems of large droplet numbers.

Generally, cellular automata do not necessarily produce the same behaviour for different spatial lattices [38]. For instance, when simulated in two or three dimensions, the earlier cellular automaton models did not correctly reproduce the curvature that is observed in the real BZ medium. Also they did not account for the dispersion relation, meaning that the medium is less excitable shortly after being excited and thus transmits excitation waves slower. These effects were captured in more recent simulations [17, 12].

Even though there are approaches of timed automata [11], there is another challenge when modelling using cellular automata: the typically fixed time steps pose additional constraints in contrast to the irregular proportions between different phases in the BZ system. This means that either the temporal resolution of the phases is coarse or that a large number of states has to be used for each phase to generate the observed timing fractions.

3.4 Discrete-Event Model for BZ Droplets

To follow the efficient simulation approach of cellular automata while including the possibility for exact timing, we propose a discrete-event based modelling and simulation approach [16]. The parameterisation of this model is relatively simple and can be derived from principal observations of the excitable medium. Furthermore, many droplet system can be simulated efficiently, i.e. many hundred excitations of systems of about 100 droplets can be simulated in less than a second. It uses coarse grained space and few discrete droplet states but continuous time. These states are the *excited*, the *refractory* and the *responsive* phase as introduced in Section 1.1 and as used by most cellular automaton approaches. Either deterministic or stochastic state transition functions can be applied, though we will only demonstrate

deterministic state transitions in this paper. We define the state transition behaviour of the droplets with the following mathematic functions:

- $\alpha(\tau)$ Probability density function for the transition time from *responsive* state to the *excited* state. Hence this parameter describes the inclination of the system to self-excite.

- $\beta(\tau)$ Probability density function for the transition time from *excited* to the *refractory* phase. Hence the length of the *excited* phase.

- $\gamma(\tau)$ Probability density function for the transition time from *refractory* to *responsive* phase. Hence the length of the *refractory* phase.

- $\psi(\tau')$ Probability density function for the transmission time of a signal from one *excited* droplet to another *responsive* droplet taking the time τ'.

For these functions, τ is the time since entering the current state. For the transmission of excitation waves, in contrast, τ' is the time needed to propagate the excitation from one droplet to another. The basic condition for transmission is that one droplet is *excited* while the other one is *responsive*. But since the spreading of waves takes some time, a delay τ' is sampled from the distribution function $\psi(\tau')$. So if one droplet is *excited* between the times t_1 and t_2, it can trigger an excitation in an adjacent droplet if this is *responsive* between $t_1 + \tau'$ and $t_2 + \tau'$.

Simulations

From an initial state of the system, all following events are sampled using the distribution functions $\alpha(\tau)$, $\beta(\tau)$, $\gamma(\tau)$ and $\psi(\tau')$. The times for these events are organised in a priority queue so that only changing droplets' states contributes to computational costs. At each simulation step, the earliest next event from the event list is selected, removed, verified and then executed by modifying the simulation data structure. Subsequently, all possible events for the modified droplet are inserted into the event queue. Events have to be verified to check if the situation of the droplet they concern has not changed in the time between issuing the event and the current simulation time. An event belonging to a droplet can for example become outdated if another droplet triggers it into an early excitation or if it is stimulated from outside the system to input data or to simulate noise. Therefore, less active or inactive parts of droplet networks do not require high computational efforts. The computational complexity of simulating a network of n droplets for a

time t scales with $O(t \cdot n \cdot log(n))$. The factor n is due to the increase in the number of events with more droplets while the logarithmic factor results from modifying the priority queue. Our simulation software can be downloaded from the project website[2].

Spatial Discretisation

An intuitive discretisation of space might be to choose one discrete droplet per position in Figure 2a, i.e. six droplets, such that the larger droplets are divided into smaller *sub-compartments*. In this case, this approach would not reproduce the observed wave dynamics:

Observing the experimental system in Section 2, the time required for excitation waves to pass from one position d_i to an adjacent one d_{i+1} is in the same order of magnitude as the oscillation period. More importantly, the wave propagation time is larger than the refractory period of about seven seconds. This means, the actually travelling excitation waves can be hidden in the signal transmission times of the discrete model. Then, an excitation wave can pass from one *sub-compartment* to another via the signal transmission delay, even if there is another excitation wave moving in the opposite direction, which would actually annihilate the first wave in the real or differential equation systems. Furthermore, cyclic oscillations can form between two *sub-compartments* when two abstract oscillations move in opposite directions without cancelling each other out. By subdividing droplets into smaller *sub-compartments*, we can choose the spatial discretisation so fine that the signal propagation time τ' becomes smaller than half of the smallest *refractory* period. This resolves the problem: Any excitation started from *sub-compartment* d_i at time t_0 will not arrive at *sub-compartment* d_{i+1} before $t_0 + \tau'$. When *sub-compartment* d_{i+1} is now sending out an opposed excitation at $t_0 + \tau' - \epsilon$, shortly before the first wave hits, d_{i+1} will clearly be refractory. The opposed wave will hit the first *sub-compartment* d_i at the earliest at time $t_0 + 2\tau' - \epsilon$, which is still before the first *sub-compartment* d_i leaves the refractory state again.

So we divided the positions up into few smaller *sub-compartments*, such that the wave propagation times for the smaller compartments are shorter than half of the refractory times as displayed in Figure 6. Hence we represent the real system of four droplets with a system of 33 discrete *sub-compartments*. Each of the positions from Figure 2a is replaced by a set of four to six *sub-compartments* for the gradual signal transmission, another two to represent the signal transmission properties of the lipid bilayer and one

[2] www.neu-n.eu

more *sub-compartment* to record the excitations at the centres of d_1 till d_6. The lipid bilayer representing *sub-compartment* are shared by two adjacent positions and are replaced by *sub-compartment* of higher excitability in the case of the contact region between positions (d_2, d_3) and (d_5, d_6), where no bilayer is present in the experiment. For the *sub-compartment* representing medium, we used a *refractory* time of six seconds, while using seven seconds for the lipid bilayer representing *sub-compartment*.

Discrete-Event Model Instances

To demonstrate the capability of the discrete-event model to reproduce the qualitative system behaviour, we show the two most prominent behaviours of the BZ droplet system presented in Section 2. To instantiate the discrete-event model in this case, we need to provide the distribution functions $\alpha(\tau)$, $\beta(\tau)$, $\gamma(\tau)$ and $\psi(\tau')$. In consistence with the differential equation models introduced before, we will only use deterministic transition functions by using the Dirac delta function $\delta(\tau - \tau_0)$. The τ_0 values will then be chosen as the timing parameters that are known from the experiments (c.f. Section 2) or could be determined from the ordinary differential equation models. In spite of the deterministic functions chosen here, it would also be possible to sample the phase transition times for example from Normal distributions, which would require the variances as further parameters though. We know that the concentration of the activating species $HBrO_2$ is noticeably high only for a very short period of time from the ordinary differential equation modelling in Section 3.1. Hence we simplify the *excited* phase to a single point in time, switching from the *responsive* to the *excited* and to the *refractory* behaviour instantly by setting $\beta(\tau) = \delta(\tau - 0)$. The transition functions for the discrete-event model *sub-compartments* as we are using them here are summarised in Table 3.

First, we simulate the dominance of the trigger waves, generated at position d_1 around experimental time 1000 s, over the remaining system in Figure 7. In simulation and approximately also in the real system, all signals are oscillations with the same periodicity as d_1 but with a shifted phase.

As second instance of the discrete model, displayed in Figure 8, we decrease the self-excitation period of position d_3 down to 6.7 s. This value is close to the oscillation periods observed between experimental times 1000 and 1200 s when a spiral wave dominates position d_2 and d_3. Furthermore, the oscillation frequency is below the 7 s refractory period that we chose for lipid-bilayer droplets, resulting in blocking at least every second trigger wave. It means that the dominance of the trigger waves from position d_1 is interrupted for positions d_4 till d_6. Instead these upper droplets are controlled by

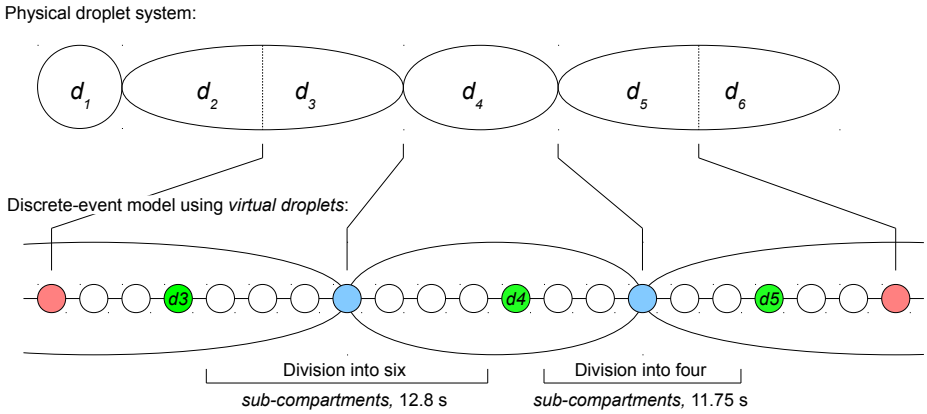

Figure 6: Mapping from the physical droplet system into the model composed of *sub-compartments*. While the upper part of the figure represents the physical droplet system as displayed in Figure 2, the lower part represents the discretisation into homogeneous and discrete *sub-compartments*. Here, the white compartments represent the actual BZ medium between the observed positions and simulate the gradual propagation of excitation waves. The coloured compartments are not delaying the wave propagation but are used for varying excitabilities and for observation. We use the blue *sub-compartments* to represent the droplet borders with their potentially higher excitability threshold that can lead to trigger waves spreading through the medium but not propagating over the lipid bilayers as observed in Section 2. The red droplets are the analogues to the blue droplets, representing the medium at the centre of the large droplets. Green droplets represent the positions d_1 ... d_6 and are introduced into the model for observing the states at these positions.

	Parameter τ_0 in $\delta(\tau - \tau_0)$ for distribution:			
	$\alpha(\tau)$	$\beta(\tau)$	$\gamma(\tau)$	$\psi(\tau)$
length of phase:	responsive	excited	refractory	transmission
d_1	0 s	0 s	8 s	0 s
d_2, d_3, d_5, d_6	9 s	0 s	6 s	0 s
d_3 normal	9 s	0 s	6 s	0 s
d_3 spiral	0.7 s	0 s	6 s	0 s
lipid bilayer droplet	8 s	0 s	7 s	0 s
medium d_1 - d_2	0 s	0 s	6 s	$\frac{10}{4}$ s
medium d_2 - d_3	9 s	0 s	6 s	$\frac{11.2}{4}$ s
medium d_3 - d_4	9 s	0 s	6 s	$\frac{12.8}{6}$ s
medium d_4 - d_5	9 s	0 s	6 s	$\frac{11.75}{4}$ s
medium d_5 - d_6	9 s	0 s	6 s	$\frac{9.8}{4}$ s

Table 3: Parameters for the discrete-event model used in the shown simulations. $\delta(\tau - \tau_0)$ denotes the Dirac delta function. The parameters are estimated from analysing the experimental data and from ordinary differential equation modelling. Parameters for droplet d_1 are chosen with a zero responsive time since we only know that it triggers excitations every eight seconds, but not if it would be possible to excite it earlier. For the signal transmission times, fractions of four and six are chosen, because the experimental droplets are subdivided into four or six smaller *sub-compartments* droplets, to reduce the otherwise large signal transmission delay. For the transmission time between position d_1 and d_2, we chose 10 s since no measurements were available here. Membrane *sub-compartments* and the lipid bilayer *sub-compartments* are parameterised with different fractions between refractory and responsive time: The lipid bilayer area seems less excitable since trigger waves that propagated through the medium could not pass over the droplet borders in the experiments.

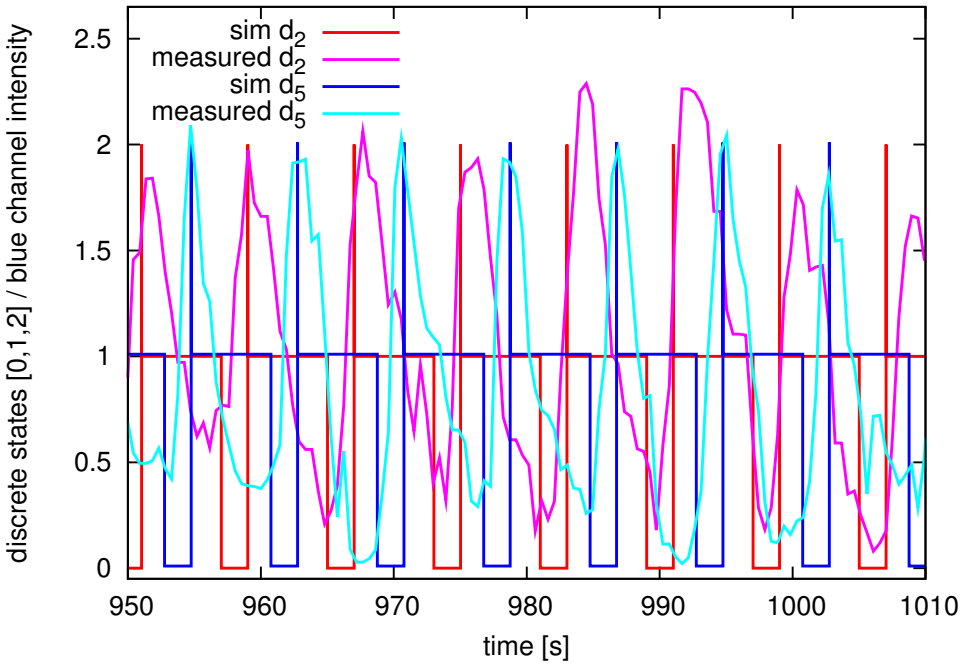

Figure 7: Comparison of the discrete model simulation for excitable droplets with the experimental system in positions d_2 and d_5 (cf.Fig. 2a). The data reflects the predominant control of the trigger waves generated by the first droplet at position d_1. The time axis for the experimental data is shifted with the function $t' = (t - 5\text{ s})$ to fit the curves of the discrete-event simulation. Furthermore, the experimental blue channel intensity is scaled to fit the interval $(0, 2)$ that is used by the discrete-event simulator to indicate the states *responsive*, *refractory* and *excited* with 0, 1 and 2 respectively. No further scaling of the time-axis was applied.

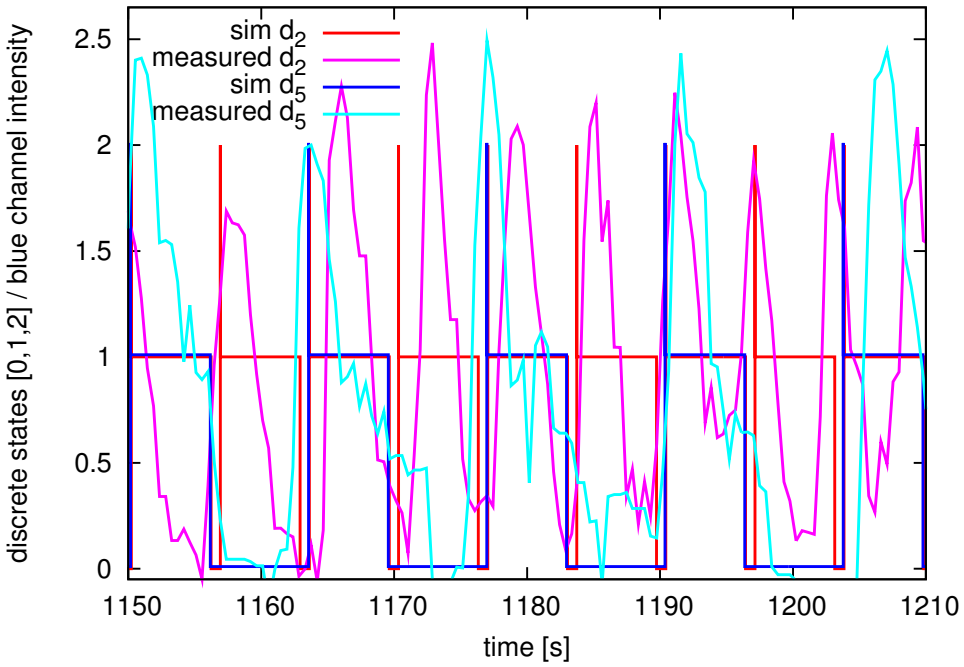

Figure 8: Comparison of the same simulation and experimental data as in the previous figure, but now at a later time-interval showing the effect of faster spiral waves in positions d_2 and d_3 on the remaining system. Since the system is modelled at time 1000 s but the related system behaviour is found around time 1200 s, the time axis for the experimental data is rescaled with the function $t' = (t * 0.95 + 57.5)$ to compensate for the lower oscillation frequency at this slightly later time of the experiment.

every second spiral wave that can pass into the third droplet at position d_4. If the period of the spiral waves was a bit longer, every second wave would not have arrived fast enough to stop positions d_4 till d_6 from self-excitation. This effect can be observed in the video (Supplementary file 1) around time 1300, when self-excitation appears in the upper droplets.

4 Modelling of Sub-Excitable Droplets

Also sub-excitable BZ droplets were modelled using partial differential equations to design small networks implementing logic and arithmetic functions that could later be used as building blocks for larger systems [25].

Logically symbolic waves are able to traverse the network modulated by interaction with pathways and other waves. The disc interior can be exploited for free space collision style reactions [5] whereas the pore loci and efficiency can compartmentalise the resulting reaction [7]. Circuits have been created from logical sub assemblies in orthogonal and hexagonal networks [25, 7]. The functional density can be increased when including more variations in relative disc size, pore efficiency and connection angles [25].

Disc designs have been simulated on a two variable version of the Oregonator model [34] as a model of the BZ reaction [46, 49] adapted for photo-sensitive modulation of the Ru-catalysed reaction [30] similar to the partial differential equation system described in Section 3.2 Use of a photo-sensitive adapted version of the Oregonator model permits a simple migration from simulation to experiment. Circuit designs from the simulation can be projected directly onto an actual photo-sensitive BZ medium [26]. Numerical simulations are achieved by integrating the equations using the Euler-ADI[3] method [36].

Contrasting previous logic gates and composite circuits designs using the BZ substrate, for example [42, 40, 32, 19], presented below are a selection of logic gates that can be created using nothing other than interconnected BZ discs. Wave fragment flow is represented by a series of superimposed time lapse images (unless stated otherwise). To improve clarity, only the activator wave front progression is recorded.

The operation of an AND gate and it's inversion, the NAND gate, are shown in Figures 9 & 10. The result of a wave collision in the NOT gate (Figure 11) was exploited to deflect and extinguish the source wave into the disc edge, whereas in the AND gate the collision between the two inputs results in 2 perpendicular fragments, one of which develops in the output cell to produce the result. A NAND gate can be created by combining the NOT gate and the AND gate (c.f. Figure 10). NAND gates are known as *universal* gates since all other gates can be created from arrangements of NAND gates alone.[4]

Essential to both adaptive behaviour in natural and synthetic computation is memory. It allows animals and machines to build an internal state

[3] Alternating direction implicit method.

[4] NOR gates are also universal gates.

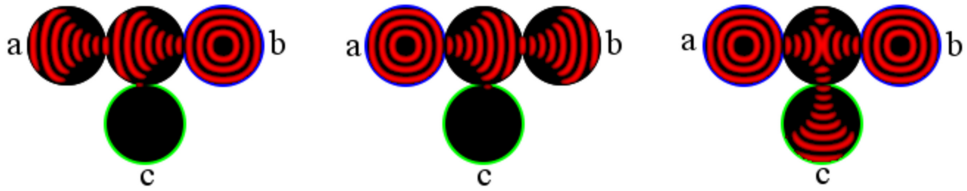

(a) $01 \rightarrow 0$ (b) $10 \rightarrow 0$ (c) $11 \rightarrow 1$

Figure 9: Two input AND gate ($\mathtt{c} = \mathtt{a} \bullet \mathtt{b}$) where inputs $\mathtt{a}, \mathtt{b}$ are top left and right discs (blue rings) and output $\mathtt{c}$ is the bottom central disc (green ring). (a) $(\mathtt{a}, \mathtt{b})(0, 1)$ A wave from input $\mathtt{b}$ propagates uninterrupted and terminates in the opposing input disc $\mathtt{a}$. (b) $(\mathtt{a}, \mathtt{b})(1, 0)$ Likewise, a wave from input $\mathtt{b}$ propagates uninterrupted and terminates in the input disc $\mathtt{b}$. (c) $(\mathtt{a}, \mathtt{b})(1, 1)$ Waves from both input discs $\mathtt{a}$ and $\mathtt{b}$ collide in the central disc and eject two perpendicular waves, one of which propagates into the output disc $\mathtt{c}$.

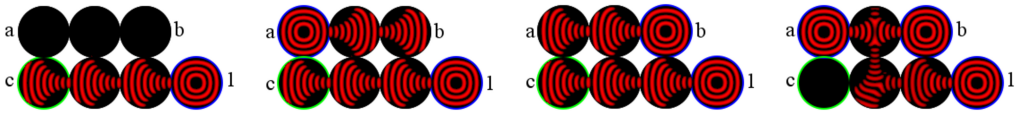

(a) 00 $\rightarrow 1$ (b) 01 $\rightarrow 1$ (c) 10 $\rightarrow 1$ (d) 11 $\rightarrow 0$

Figure 10: Two input NAND gate ($\mathtt{c} = \overline{\mathtt{a} \bullet \mathtt{b}}$) where inputs $\mathtt{a}, \mathtt{b}$ are top left and right discs (blue rings) and output $\mathtt{c}$ is the bottom left disc (green ring), source input is located on the bottom right (blue ring). Operation is identical to the AND gate (Figure 9) but with an inverter (Figure 11) integrated along the bottom disc row. (a), (b) & (c) The source input provides a logical '1' output for all input combinations other than $(\mathtt{a}, \mathtt{b})(1, 1)$. (d) $(\mathtt{a}, \mathtt{b})(1, 1)$ Output from the AND gate portion of the gate collides with the source input creating a logical '0' output.

independent from the current external world state. We present an example 1 bit volatile read write memory cell constructed entirely with BZ discs. Independent but similar to previous designs [32, 33] in so much that the existence or absence of a rotating wave represents the setting or resetting of 1 bit of information.

When two BZ waves progress in opposite directions around an enclosed channel, loop or ring of connected discs, then at some point the two opposing wave fronts will meet and are always mutually annihilated. Nevertheless, if a unidirectional wave can be inserted into the loop then that wave front will

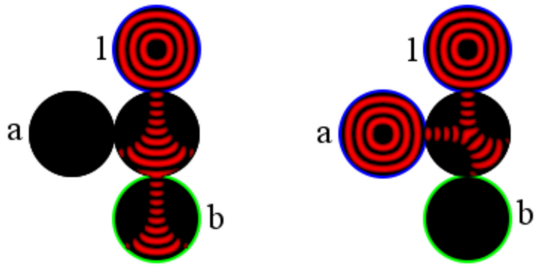

(a) $0 \rightarrow 1$ (b) $1 \rightarrow 0$

Figure 11: Inverter gate ($\mathtt{a} = \overline{\mathtt{b}}$) where the input $\mathtt{a}$ is centre left (blue ring), bottom disc (green ring) is the output $\mathtt{b}$ and a supply, or source logical '1' top most disk (blue ring). (a) $\mathtt{a} = 0$ The gate initiates with the source pulse in the top disc. In this case, no signal is present at the input disc and the source pulse travels to the output disc (bottom) resulting in a logical 1 output ($1 \rightarrow 0$). (b) $\mathtt{a} = 1$ Again the source pulse travels from top to bottom, but in this case a collision with a signal present on the input disc produces a logical 0 output. ($0 \rightarrow 1$).

rotate around the loop indefinitely[5]. Furthermore the rotating wave can be terminated by the injection of another asynchronous wave rotating in the opposite direction. Opposing inputs into a loop are analogous to a memory *set* or *reset*. Reading the state of the cell without changing the state can be achieved by connecting another output node where a stream of pulses can be directed to modulate other circuits [20] (Figure 12).

The loop and a unidirectional gate (diode) are the two key constructions of this type of memory cell. Unidirectional gates in BZ media have previously been created by exploiting asymmetric geometries or chemistry on either side of a barrier [9]. An alternative design is possible however using discs connected with different apertures. The operation relies on the relationship between the wave expansion and the angle of the connection. Fine control of the wave beam would in theory allow other angles of connectivity [6] and other functions.

5 Outlook

Next to generating reusable logic gate designs in Section 4, we will further exemplify the use and necessity for models on different scales by showing

[5]For as long as the chemical reagents can sustain the reaction.

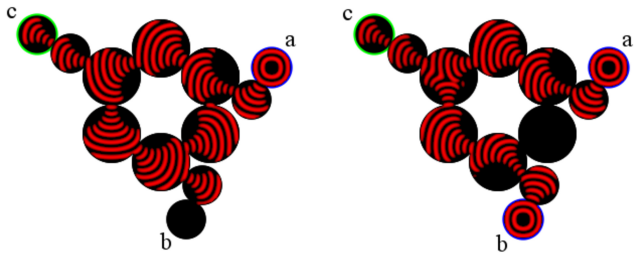

(a) (b)

Figure 12: Memory cell with additional diodes on the cell inputs. Two additional angled diode junctions are added to each of the input discs (`a` & `b`). This prevents a reverse wave flow back down either of the inputs. An example output disc is also connected (top left). (a) Wave insertion at (top right) `a` input node results in a persistent counter-clockwise wave. Reverse wave flow down the opposing (bottom) input is blocked by an angled diode junction. (b) Simultaneous `a` & `b` inputs produce one output pulse `c` and annihilate wave rotation.

an outlook into our currently ongoing research. This research on computing droplet systems heavily depends on the presented droplet models and their simulation.

5.1 Conventional Circuit Designs from Logic Gates

Even though networks of conventional binary logic gates might not be the ideal application for droplet based computing, the simplicity of writing down binary logic formulas might lead to some important applications such as smart drugs, which could already benefit of implementing even simple logics.

As a simple example of a larger sized droplet system using binary logic, the "input counter" network is shown in Figure 13. It encodes inputs and outputs to and from the network through the absence or presence of excitations. It discriminates between zero, one, two or three inputs that are stimulated independently. In response, it should always stimulate exactly one out of four possible output lanes maximally, dependent on the number of activated inputs.

The connectivity of the network is displayed in Figure 13a and leads to the 3d structure of the network that is displayed in Figure 13b when fed into the simulator. Noticeably the schematic graph uses droplet connections that cross over, effectively necessitating a three dimensional implementation

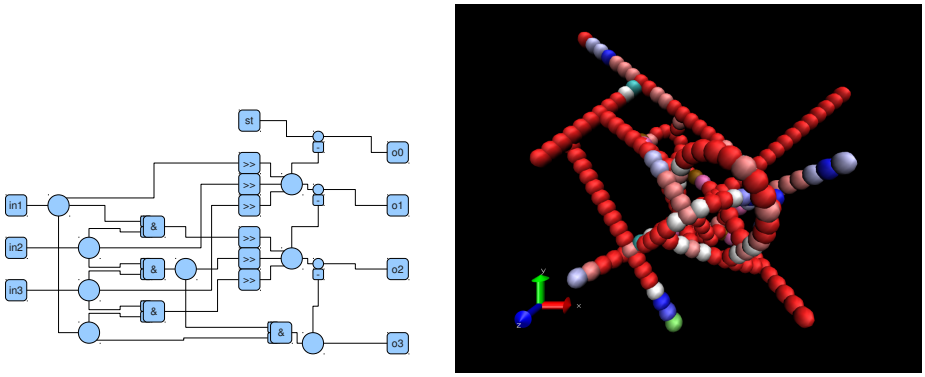

(a) Network Schematic (b) Network Simulation

Figure 13: A counting droplet network as design and in simulation. Dependent on the number of stimulated inputs, four different outputs will be excited maximally, representing the sum of the stimulated channels. a) Schematic of the droplet circuit using *Or*, *High Activity* and the postulated *And*, *Repeater*, *Diode* and *Inhibition* droplet types. b) The three dimensional implementation of the network design is shown with red droplets denoting *responsive* medium, while the white and blue tones represent the excited and refractory states.

of the droplet system that we cannot yet produce experimentally.

5.2 Evolutionary Design of Droplet Networks

Next to engineering approaches for designing computing droplet networks, we are investigating different "programming" schemes. Using evolutionary algorithms, we do not specify how the problems should be solved but what properties the solution to the problems should posses. To this aim a fitness function is specified that evaluates how close a droplet design fulfils the requirements. This means that the specified demands do not have to be confined to the correct production of results but can among others also involve the size of the solution droplet network or its robustness against noise. The fitness evaluation is most likely implemented via simulation, at least in the first steps, until a set of candidates solutions emerge that can be tested experimentally.

We also study spontaneous formation of networks composed by droplets exhibiting local interactions, whose architectures are able to compute. Computability is here measured qualitatively in terms of network's competence to reach to specific states, as well as quantitatively, using information theory

measures to evaluate its operational capacities. Moreover, we analyse the role of selection pressure when evolving such architectures. In a first attempt to simulate this process, the developing spatial configuration is regulated by the localisation and states of the droplets and their interactions. Later, we apply external signals as perturbations that trigger phase changes in droplets, possibly generating reorganisations in the network (and hopefully self-healing actions). These events are then used to understand how to control in some way the process of development and also determine the robustness of the system.

From another point of view, not only the structures of droplet networks matters but also the encoding of signals that are fed into it, i.e. as input data or parameter to any kind of computation. To this aim we investigated the combined evolution of stimulation patterns and droplet network structures for computing simple binary functions in [23] as displayed in Figure 14.

In an exemplary futuristic application, droplet networks could be used as "intelligent" drugs that could be activated under very specific conditions. So we are for example evolving classifiers for biomarkers, e.g. from the benchmarking dataset Proben1 [35].

6 Conclusions

In this paper we presented a summary on current techniques of modelling compartmentalised excitable media exemplified with lipid covered droplets of Belousov-Zhabotinsky BZ medium swimming in oil. Accompanied by an experimental system of four droplets and analysing their behaviour over a time of about 48 minutes during which we registered about 300 oscillations waves. Starting from a non-spatial ordinary differential equation model, a spatial perspective is reviewed in the partial differential equation models. Then, spatial and temporal discretisation is to speed up simulation studies using cellular automata is discussed. Finally, in the Sections 3.4, an event-based model is proposed to achieve higher timing precision while preserving the efficiency for the investigation of large systems.

Even though we showed the qualitative reproduction of the systems behaviour with the discrete-event model, there are some effects that are not yet covered by this approach. Most obviously, the oscillation periods are increasing over the experimental times up to a factor of about three. This is neither covered by the differential equations nor by the discrete droplet models. While we are currently working on extending the differential equation systems to include this effect, it might in principle be easier to reproduce this effect in the more phenomenological event-based systems by adding the

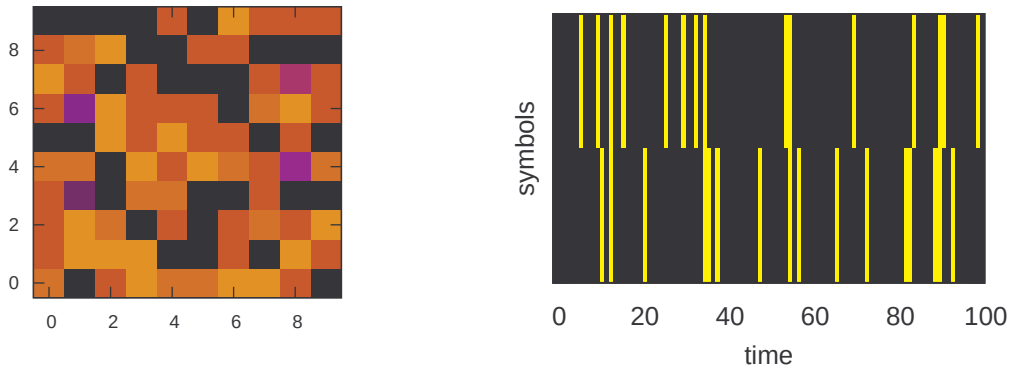

(a) Evolved Droplet Network

(b) Evolved Signal Encoding

Figure 14: Evolution of droplet networks topologies in combination with symbol encoding patterns. (a) Rendering of an evolved droplet network instance. Each square represents a droplet on a two dimensional array. Black cells represent empty spaces that are not excitable, different red tones represent different species of excitable droplets that were modified by an evolutionary algorithm. The four blue cells represent fixed input / output droplets. A von Neumann neighbourhood around each cell defines the connectivity of the droplets, i.e. droplets that are directly on top, bottom, left or right are connected and can excite one another.
(b) Example of two symbols that evolved together with a network instance to realize the XOR function. The lower row of the image represents symbol '0' while the upper row represents symbol '1'. Time advances in x direction over 100 frames where the input droplets of (a) are stimulated only in the intervals that are represented by yellow vertical bars.

global time t as another parameter, such that the probability distribution functions look like $\alpha(t,\tau)$, $\beta(t,\tau)$, $\gamma(t,\tau)$ and $\psi(t,\tau')$. Furthermore, the dispersion relation [29, 17] is another currently neglected effect, meaning that excitation waves move faster when the medium had more time to recover after the previous excitation. Here partial differential equation approaches already capture this effect but it would also be possible have a signal transmission function $\psi(\tau')$ that considers the droplets excitation history.

Observing the experimental data of Figure 2c, it becomes clear that a certain level of noise is part of the system, even though some quantum of the noise will also be due to the camera and digitalisation process. So we expect some uncertainty about the length of the oscillation period [10], about the length of its phases, about the amplitudes, about the geometries of droplets, about the excitability of droplets and about the connectivity between droplets. These effects are probably rather troublesome properties of the system that will make the design of robustly working droplet computers more challenging. Consequently, a useful model of computing droplets systems will have to consider random perturbations. Though we do not show how to estimate the correct noise levels from the experiments here, especially the discrete models allow a parameterisation of the transition functions, e.g. by representing the fluctuations as Gaussian probability density functions instead of the Dirac delta function.

Acknowledgements

The research was supported by the NEUNEU project (248992) sponsored by the European Community within FP7-ICT-2009-4 ICT-4-8.3 - FET Proactive 3: Bio-chemistry-based Information Technology (CHEM-IT) program.

Supplementary Material

- Supplementary movie 1: `droplet_chain_1_1.mpg` can be downloaded from the project website:
  `http://www.chemicalneuronalnet.uni-jena.de/neuneu_media/de/MoviesAndPictures/droplet_chain_1_1.mpg` and shows the experiment described in Section 2.

References

[1] A. Adamatzky. *Computing in nonlinear media and automata collectives*. Institute of Physics Publishing, 2001.

[2] A. Adamatzky. *Collision-based computing*. Springer Verlag, 2002.

[3] A. Adamatzky. Collision-based computing in belousov-zhabotinsky medium. *Chaos, Solitons & Fractals*, 21(5):1259–1264, 2004.

[4] A. Adamatzky. On excitable beta-skeletons. *Journal of Computational Science*, 1(3):175 – 186, 2010.

[5] A. Adamatzky and B. Costello. Experimental logical gates in a reaction-diffusion medium: The xor gate and beyond. *Physical Review E*, 66(4): 046112, 2002.

[6] A. Adamatzky, B. de Lacy Costello, and L. Bull. On polymorphic logical gates in sub-excitable chemical medium. *International Journal of Bifurcation and Chaos*, 21(7):1977–1986, 2011.

[7] A. Adamatzky, B. De Lacy Costello, L. Bull, and J. Holley. Towards arithmetic circuits in sub-excitable chemical media. *Israel Journal of Chemistry*, 51(1):56–66, 2011.

[8] S. Aghdaei, M. Sandison, M. Zagnoni, N. Green, and H. Morgan. Formation of artificial lipid bilayers using droplet dielectrophoresis. *Lab Chip*, 8(10):1617–1620, 2008.

[9] K. Agladze, R. Aliev, T. Yamaguchi, and K. Yoshikawa. Chemical diode. *The Journal of Physical Chemistry*, 100(33):13895–13897, 1996.

[10] F. Ali and M. Menzinger. Stirring effects and phase-dependent inhomogeneity in chemical oscillations: The belousov-zhabotinsky reaction in a cstr. *The Journal of Physical Chemistry A*, 101(12):2304–2309, 1997.

[11] R. Alur and D. L. Dill. A theory of timed automata. *Theoretical Computer Science*, 126(2):183–235, 1994.

[12] D. Barkley. A model for fast computer simulation of waves in excitable media. *Physica D: Nonlinear Phenomena*, 49(1-2):61–70, 1991.

[13] P. Dittrich. *LNCS 3566 - Unconventional Programming Paradigms (UPP 2004)*, chapter Chemical Computing, pages 19 – 32. Springer, Berlin, 2005.

[14] P. Dittrich, J. Ziegler, and W. Banzhaf. Artificial chemistries–a review. *Artif Life*, 7(3):225–275, 2001.

[15] R. Field, E. Körös, and R. Noyes. Oscillations in chemical systems. II. Thorough analysis of temporal oscillation in the bromate-cerium-malonic acid system. *Journal of the American Chemical Society*, 94 (25):8649–8664, 1972.

[16] G. Fishman. *Discrete-Event Simulation: Modeling, Programming, and Analysis*. Springer Verlag, 2001.

[17] M. Gerhardt, H. Schuster, and J. Tyson. A cellular automation model of excitable media including curvature and dispersion. *Science*, 247(4950): 1563, 1990.

[18] J. N. Gorecka, J. Gorecki, J. Szymanski, and K. Gizynski. A simple model of interactions between belousov-zhabotinsky droplets. *not yet published*, 2012.

[19] J. Gorecki and J. Gorecka. *Computing in Geometrical Constrained Excitable Chemical Systems*, pages 1352–1376. Springer-Verlag, 2009.

[20] J. Gorecki, K. Yoshikawa, and Y. Igarashi. On chemical reactors that can count. *The Journal of Physical Chemistry A*, 107(10):1664–1669, 2003.

[21] J. Gorecki, J. Szymanski, and J. N. Gorecka. Realistic parameters for simple models of the belousov–zhabotinsky reaction. *The Journal of Physical Chemistry A*, 115(32):8855–8859, 2011.

[22] J. M. Greenberg and S. P. Hastings. Spatial patterns for discrete models of diffusion in excitable media. *SIAM Journal on Applied Mathematics*, 34(3):pp. 515–523, 1978.

[23] G. Gruenert, G. Escuela, and P. Dittrich. Symbol representations in evolving droplet computers. *NEUNEU Technical Report*, 2012.

[24] L. Gyorgyi, T. Turànyi, and R. Field. Mechanistic details of the oscillatory belousov-zhabotinskii reaction. *Journal of physical chemistry*, 94 (18):7162–7170, 1990.

[25] J. Holley, A. Adamatzky, L. Bull, B. De Lacy Costello, and I. Jahan. Computational modalities of belousov-zhabotinsky encapsulated vesicles. *Nano Communication Networks*, 2:50–61, 2011.

[26] J. Holley, I. Jahan, B. Costello, L. Bull, and A. Adamatzky. Logical and arithmetic circuits in belousov zhabotinsky encapsulated discs. *Physical Review E*, 84(5):056110, 2011.

[27] M.-T. Hütt, M. K. Jain, C. C. Hilgetag, and A. Lesne. Stochastic resonance in discrete excitable dynamics on graphs. *Chaos, Solitons & Fractals*, (0):–, 2012.

[28] M. Januszewski and M. Kostur. Accelerating numerical solution of stochastic differential equations with cuda. *Computer Physics Communications*, 181(1):183 – 188, 2010.

[29] J. P. Keener and J. J. Tyson. Spiral waves in the Belousov-Zhabotinskii reaction. *Physica D: Nonlinear Phenomena*, 21(2-3):307–324, Sept. 1986.

[30] L. Kuhnert. A new optical photochemical memory device in a light-sensitive chemical active medium. *Nature*, 319:393, 1986.

[31] G. Maglia, A. Heron, W. Hwang, M. Holden, E. Mikhailova, Q. Li, S. Cheley, and H. Bayley. Droplet networks with incorporated protein diodes show collective properties. *Nature Nanotechnology*, 4(7):437–440, 2009.

[32] I. Motoike and K. Yoshikawa. Information operations with an excitable field. *Physical Review E*, 59(5):5354, 1999.

[33] I. Motoike, K. Yoshikawa, Y. Iguchi, and S. Nakata. Real-time memory on an excitable field. *Physical Review E*, 63(3):036220, 2001.

[34] R. Noyes, R. Field, and E. Koros. Oscillations in chemical systems. i. detailed mechanism in a system showing temporal oscillations. *Journal of the American Chemical Society*, 94(4):1394–1395, 1972.

[35] L. Prechelt et al. Proben1: A set of neural network benchmark problems and benchmarking rules. *Fakultät für Informatik, Univ. Karlsruhe, Karlsruhe, Germany, Tech. Rep*, 21:94, 1994.

[36] W. Press, B. Flannery, S. Teukolsky, and W. Vetterling. *Numerical Recipes in C: The Art of Scientific Computing*. Cambridge University Press, England, 2nd edition, 1992.

[37] I. Prigogine and R. Lefever. Symmetry breaking instabilities in dissipative systems. ii. *The Journal of Chemical Physics*, 48(4):1695–1700, 1968.

[38] T. S. Shimizu, S. V. Aksenov, and D. Bray. A spatially extended stochastic model of the bacterial chemotaxis signalling pathway. *J Mol Biol*, 329(2):291–309, May 2003.

[39] O. Steinbock and S. Müller. Radius-dependent inhibition and activation of chemical oscillations in small droplets. *The Journal of Physical Chemistry A*, 102(32):6485–6490, 1998.

[40] O. Steinbock, P. Kettunen, and K. Showalter. Chemical wave logic gates. *The Journal of Physical Chemistry*, 100(49):18970–18975, 1996.

[41] J. Szymanski, J. N. Gorecka, Y. Igarashi, K. Gizynski, J. Gorecki, K.-P. Zauner, and M. D. Planque. Droplets with information processing ability. *International Journal of Unconventional Computing*, 2011.

[42] Á. Tóth and K. Showalter. Logic gates in excitable media. *The Journal of chemical physics*, 103:2058, 1995.

[43] J. von Neumann. *Theory of Self-Reproducing Automata*. University of Illinois Press, Champaign, IL, USA, 1966.

[44] A. T. Winfree. Spiral waves of chemical activity. *Science*, 175(4022): 634–636, 1972.

[45] S. Wolfram. Statistical mechanics of cellular automata. *Reviews of Modern Physics*, 55(3):601–644, July 1983.

[46] A. Zaikin and A. Zhabotinsky. Concentration wave propagation in two-dimensional liquid-phase self-oscillating system. *Nature*, 225(5232):535–537, 1970.

[47] A. N. Zaikin and A. M. Zhabotinsky. Concentration wave propagation in two-dimensional liquid-phase self-oscillating system. *Nature*, 225(5232): 535–537, Feb. 1970.

[48] K. Zauner. Molecular information technology. *Critical reviews in solid state and materials sciences*, 30(1):33, 2005.

[49] A. Zhabotinsky and A. Zaikin. Autowave processes in a distributed chemical system. *Journal of theoretical biology*, 40(1):45–61, 1973.